

Chiral polaritons in semiconductor perovskite metasurface enhanced by bound states in the continuum

Dun Wang(汪顿), Albert Y. Xiong), Julia Q. Zhang), Zengde She(佘增德), Xiaofeng Kang(康晓峰), Ying Zhu(朱莹), Sanjib Ghosh), and Qihua Xiong(熊启华)
Citation: Chin. Phys. B, 2024, 33 (**12**): 128103. DOI: 10.1088/1674-1056/ad8db5
Journal homepage: http://cpb.iphy.ac.cn; http://iopscience.iop.org/cpb

What follows is a list of articles you may be interested in

Transmissive 2-bit anisotropic coding metasurface

Pengtao Lai(来鹏涛), Zenglin Li(李增霖), Wei Wang(王炜), Jia Qu(曲嘉), Liangwei Wu(吴良威),Tingting Lv(吕婷婷), Bo Lv(吕博), Zheng Zhu(朱正), Yuxiang Li(李玉祥),Chunying Guan(关春颖), Huifeng Ma(马慧锋), and Jinhui Shi(史金辉)
Chin. Phys. B, 2022, 31 (**9**): 098102. DOI: 10.1088/1674-1056/ac4a6b

Multiple bottle beams based on metasurface optical field modulation and their capture of multiple atoms

Xichun Zhang(张希纯), Wensheng Fu(付文升), Jinguang Lv(吕金光), Chong Zhang(张崇),Xin Zhao(赵鑫), Weiyan Li(李卫岩), and He Zhang(张贺)
Chin. Phys. B, 2022, 31 (**8**): 088103. DOI: 10.1088/1674-1056/ac4e06

High efficiency and broad bandwidth terahertz vortex beam generation based on ultra-thin transmission Pancharatnam-Berry metasurfaces

Wenyu Li(李文宇), Guozhong Zhao(赵国忠), Tianhua Meng(孟田华), Ran Sun(孙然), and Jiaoyan Guo(郭姣艳)
Chin. Phys. B, 2021, 30 (**5**): 058103. DOI: 10.1088/1674-1056/abd75c

Ultra-wideband reflective polarization converter based on anisotropic metasurface

Jia-Liang Wu(吴家梁), Bao-Qin Lin(林宝勤), Xin-Yu Da(达新宇)
Chin. Phys. B, 2016, 25 (**8**): 088101. DOI: 10.1088/1674-1056/25/8/088101

Polarization-insensitive unidirectional spoof surface plasmon polaritons coupling by gradient metasurface

Hong-yu Shi(施宏宇), An-xue Zhang(张安学), Jian-zhong Chen(陈建忠), Jia-fu Wang(王甲富), Song Xia(夏颂), Zhuo Xu(徐卓)
Chin. Phys. B, 2016, 25 (**7**): 078105. DOI: 10.1088/1674-1056/25/7/078105

RAPID COMMUNICATION

Chiral polaritons in semiconductor perovskite metasurface enhanced by bound states in the continuum

Dun Wang(汪顿)[1], Albert Y. Xiong[2], Julia Q. Zhang[2], Zengde She(佘增德)[1], Xiaofeng Kang(康晓峰)[2], Ying Zhu(朱莹)[2], Sanjib Ghosh[3], and Qihua Xiong(熊启华)[1,2,3,4,†]

[1] *State Key Laboratory of Low-Dimensional Quantum Physics, Department of Physics, Tsinghua University, Beijing* 100084, *China*
[2] *Tsinghua International School, Beijing* 100084, *China*
[3] *Beijing Academy of Quantum Information Sciences, Beijing* 100193, *China*
[4] *Frontier Science Center for Quantum Information, Beijing* 100084, *China*

(Received 27 September 2024; revised manuscript received 30 October 2024; accepted manuscript online 1 November 2024)

The exploration of novel chiral optical platforms holds both fundamental and practical importances, which have shown great promise towards applications in valleytronics, chiral sensing and nanoscopic chiroptics. In this work, we combine two key concepts — chiral bound states in the continuum and exciton polaritons — to showcase a strong chiral response from polaritons. Using the finite element method, we numerically design a $CsPbBr_3$ based metasurface that supports intrinsically chiral bound states in the continuum and verify the chirality by calculating the reflection spectrum and eigen-polarization mapping. We further demonstrate chirality-dependent exciton polariton angular dispersion arising from the strong coupling between the chiral BIC and excitons in $CsPbBr_3$ by simulating the polariton angle-resolved absorption spectrum. Reciprocity analysis reveals that the polariton photoluminescence in different momentum space locations is selectively enhanced by chiral pumping light. Our results suggest a promising first step towards chiral polaritonics.

Keywords: bound states in the continuum, chirality, metasurface, perovskite microcavities, exciton polariton

PACS: 81.05.Xj, 71.35.–y, 71.36.+c, 78.20.Bh **DOI:** 10.1088/1674-1056/ad8db5

1. Introduction

Chirality refers to the property that an object cannot be brought to coincide with its mirror image by translation and rotation operations.[1] In the field of chiral optics, the left circularly polarized (LCP) and right circularly polarized (RCP) states of light are mirror images of each other, carrying photon spin angular momenta of $+\hbar$ and $-\hbar$, respectively, and interact differently with chiral particles or structures. Chiral light has found wide applications ranging from topological photonics,[2] quantum computing,[3] valleytronics[4] to biological sensing[5] and chemical synthesis.[6] Therefore, one of the major challenges in contemporary optics is to realize chiral light sources with high degree of polarization on ultra-compact, integrable nanostructures.[7] Many approaches have been attempted for this purpose. Some molecules possess natural chirality, but the interaction between these molecules and chiral light is often very weak, limiting their use in practical applications.[1] Methods such as spin injection[8,9] and external electromagnetic field control[10] are also frequently used to generate chiral light and have made solid progress in recent years. With the development of micro-nano material processing, the fabrication of metal and dielectric chiral microcavities has become possible and is now receiving increasing attention. Highly pure chiral response and chiral lasing from optical metasurfaces have been achieved through polarization conversion[11,12] and Pancharatnam–Berry phase engineering, introduced by spin–orbit coupling.[13,14] However, those existing strategies still face issues such as low energy conversion efficiency, low quality factor (Q factor), and chirality appearing only at specific large angles.

In the past decade, the concept of "bound states in the continuum" (BIC) has become a prominent presence in the optics community.[15] These photonic modes have energies lying in the allowed bands, but their electromagnetic fields are completely confined within the resonant structure, unable to radiate energy outward or be excited by electromagnetic waves from free space, thus exhibiting ultralong photon lifetimes and diverging Q values. By varying structural parameters, BIC can be transformed into quasi-BIC (qBIC) with a very high but finite Q value that enables coupling to free space radiation, which is essential for device applications. The unique characteristics of BIC and qBIC have been explored to realize many interesting phenomena such as unidirectional waveguide resonances,[16] vortex beam generation,[17] optical spin Hall effects,[18] enhancing the Goos–Hänchen shift,[19] suppressing radiation loss in metal–dielectric systems,[20] and high harmonic generation.[21] After the first observation of BIC in photonic structures, a series of studies have indicated that BIC can be regarded as a topological singularity in momentum space with an integer topological charge;[22] when the in-plane

†Corresponding author. E-mail: qihua_xiong@tsinghua.edu.cn
© 2024 Chinese Physical Society and IOP Publishing Ltd

symmetry is broken, a BIC splits into two (or more) qBICs with half-integer charges, which appear as circular polarization states that only couple with one circular polarization (thus also called C points or chiral BIC), opening up the possibility of using BIC in chiral optical devices.[23–25] Furthermore, recent studies have shown that by breaking the out-of-plane mirror symmetry, the position of chiral BIC in momentum space can be manipulated to simultaneously control the polarization texture, emission angle and Q value, making BIC an attractive platform for chiral optics research.[26,27] It should be mentioned that BIC can be levered to manipulate not only the spin angular momentum (polarization) but the orbital angular momentum.[28]

On the other hand, the strongly localized electric field and long photon lifetime provided by BIC can significantly enhance light–matter interaction, without using bulky vertical microcavities. Therefore, there has been extensive research effort in coupling BIC with material excitations. In the weak coupling regime, the small mode volume of the BIC light field guarantees a larger Purcell factor, thereby enhancing the luminescence of excitons[29] or single-photon sources[30] in two-dimensional materials. In the strong coupling regime, coherent energy exchange between excitons in semiconductor materials and photons leads to the formation of a new kind of quasi-particle — exciton polaritons. Thanks to the bosonic nature and half light, half matter properties, exciton polaritons serve as an excellent platform for realizing room-temperature Bose–Einstein condensation, ultrafast optical switches, all-optical quantum simulation, and other novel phenomena and applications.[31] Due to its ultralong photon lifetime and extreme field confinement, BIC is naturally advantageous for achieving strong coupling, and it is expected that BIC in periodic structures holds great potentials for exciton polariton research. Numerical simulations and experimental studies have observed strong coupling between one-dimensional BIC gratings and perovskites, as well as two-dimensional transition metal dichalcogenides (TMDs), and in these cases the Rabi splitting can be significantly larger than previous results from planar microcavities or photonic crystal cavities.[32–34] In 2022, V. Ardizzone *et al.* first observed the condensation of exciton polaritons on a BIC ground state in a GaAs multilayer quantum well structure at low temperatures,[35] and subsequently, other research groups also reported BIC polariton condensation at room temperature based on two-dimensional silicon and perovskite metasurfaces.[36,37] However, strong coupling between chiral BIC and excitons has not yet been fully explored, where the pure chirality and high Q factor of chiral BIC could be imparted to the photoluminescence (PL) of exciton polaritons, enabling chiral control of exciton polaritons. This system could be a promising candidate for a chiral laser that combines room temperature operation, low threshold, vertical emission, high Q factor, and pure circularly polarized light.

Among various polaritonic materials, lead-halide perovskites stand out due to their stable excitons at room temperature, high optical gain, strong oscillator strength, tunable band structure, and mature growth techniques.[31,38] In this work, we use finite element method (FEM) numerical simulations to design an inorganic $CsPbBr_3$ perovskite metasurface that supports an intrinsic chiral BIC. Through calculation of the photonic band structure and eigenpolarization mapping, the evolution of chiral BIC is illustrated in detail and strong intrinsic chirality ($|S_3/S_0 > 0.99|$) and a Q factor of over 20000 are simultaneously demonstrated. Contribution of the toroidal dipole resonance is identified in the multipole analysis. Strong coupling between chiral BIC and perovskite excitons is revealed in angle and polarization-resolved reflection and absorption spectra, observing a Rabi splitting of over 100 meV and distinct exciton polariton chiral response. Simulated PL spectrum also shows intrinsic chiral emission enhancement, which implies potential chirality-dependent condensation and propagation behavior.

2. Design and characterization of the chiral BIC

The geometry of our metasurface design is shown in Fig. 1. The inorganic perovskite $CsPbBr_3$ is formed into a square lattice with period $a = 325$ nm. The perovskite is grown on a 1 μm SiO_2/Si substrate, and a layer of 400 nm thick poly(methyl methacrylate) (PMMA) is coated on top for both protection and refractive index matching with SiO_2.[34] The unit cell is based on a cylindrical hole with height $H = 120$ nm and radius $R = 80$ nm (Fig. 1(b)), along with two geometric perturbations: a rectangular slot having dimensions $W = 60$ nm, $L = 70$ nm and protruding at 135° angle with x axis (Fig. 1(c)), and a tilting angle $\theta = 18°$ towards the 45° direction in xy plane (Fig. 1(d)). For brevity, we will rename the 45° and 135° directions x' and y' axes, respectively, as labeled in Fig. 1(c).

In general, there are two kinds of loss mechanisms in such a photonic structure: radiation loss, by which energy leaks out into free space at a rate γ_r, and material loss, by which energy is absorbed by the material itself at a rate γ_i. The former happens in the case of leaky resonances, which can be solved as eigenmodes of a Hamiltonian with a real dielectric function $\varepsilon(\omega)$ under semi-infinite boundaries, while the latter originates from the interaction of material excitations with light and is described by the imaginary part of $\varepsilon(\omega)$. As the distinction between BIC and qBIC lies in whether γ_r vanishes, we apply a two-step strategy in our design. In the first step treated in this section, only the radiation loss is considered and we replace the dielectric function of $CsPbBr_3$ with its off-resonance

real value[39] $\varepsilon = n^2 = 2.25^2$. We assume here that the perovskite is grown with in-plane a and b crystallographic axes so that the refractive index is isotropic and contributes negligibly to symmetry breaking.[39] In the second step treated in the next section, we will include the exciton resonance into $\varepsilon(\omega)$. The commercial softwares COMSOL Multiphysics and Ansys Lumerical are employed for numerical simulations, using the finite element method to solve Maxwell's equations and obtain the system's eigenmodes and spectral features. In COMSOL Multiphysics, the "Electromagnetic Waves, Frequency Domain" interface from the RF module is used to solve for the eigenmodes and reflection spectra. In Ansys Lumerical, we use the finite-difference time-domain (FDTD) suite to calculate the angle-resolved spectra. The simulation domain is defined as a unit cell with Bloch boundary conditions applied in the x and y directions, and sufficiently thick perfectly matched layers (PML) are added in the z direction to simulate semi-infinite space. The mesh in the active region is set to have a resolution of approximately 10 nm to ensure accurate simulation of high Q resonances. Spectral responses are computed under plane wave incidence (port boundary condition in COMSOL) and angle-resolved spectra are obtained by varying the incident angles. The incident light source is positioned 1 μm above the structure; for the visible wavelengths considered, this distance is sufficient to avoid the influence of near-field effects.

Our analysis starts with the leaky modes in the unperturbed structure of Fig. 1(b). The angle-resolved reflection spectrum along x is shown in Fig. 2(a), where four optical modes can be identified within the energy range of interest, labeled as modes 1, 2, 3, and 4 from the highest to lowest energy. The broad resonances near 2.2 eV are far from the energy of interest (exciton energy in $CsPbBr_3$, which is about 2.4 eV) and do not significantly affect the subsequent results. Modes 1 and 4 have linewidths decreasing to 0 at the Γ point, where they become BIC dark states that cannot be excited by incident light. The bright modes 2 and 3 are degenerate at Γ, while the BICs 1 and 4 are non-degenerate, which agree with the symmetry characteristics of BICs. The quality factors of both BICs diverge at the Γ point, as shown in Fig. 2(b), satisfying the general scaling relation $Q \propto |k_x|^{-2}$. An important difference between the BIC modes 1 and 4 is that the energy-momentum dispersion is parabola-like for mode 1 while inverted parabola-like for mode 4 (Fig. 2(a)). In a square lattice, the dispersion along y is the same as that along x. Consequently, only mode 1 can be occupied by lower branch exciton polaritons in the strong coupling regime, so we focus on the properties of this mode. Its electric and magnetic field in xy plane is plotted in Fig. 2(c). Mode 1 has a C_4^z symmetry with field hotspots at the unit cell corners, thus it will be more sensitive to perturbations installed along x' and y' directions, as we do in Figs. 1(c) and 1(d).

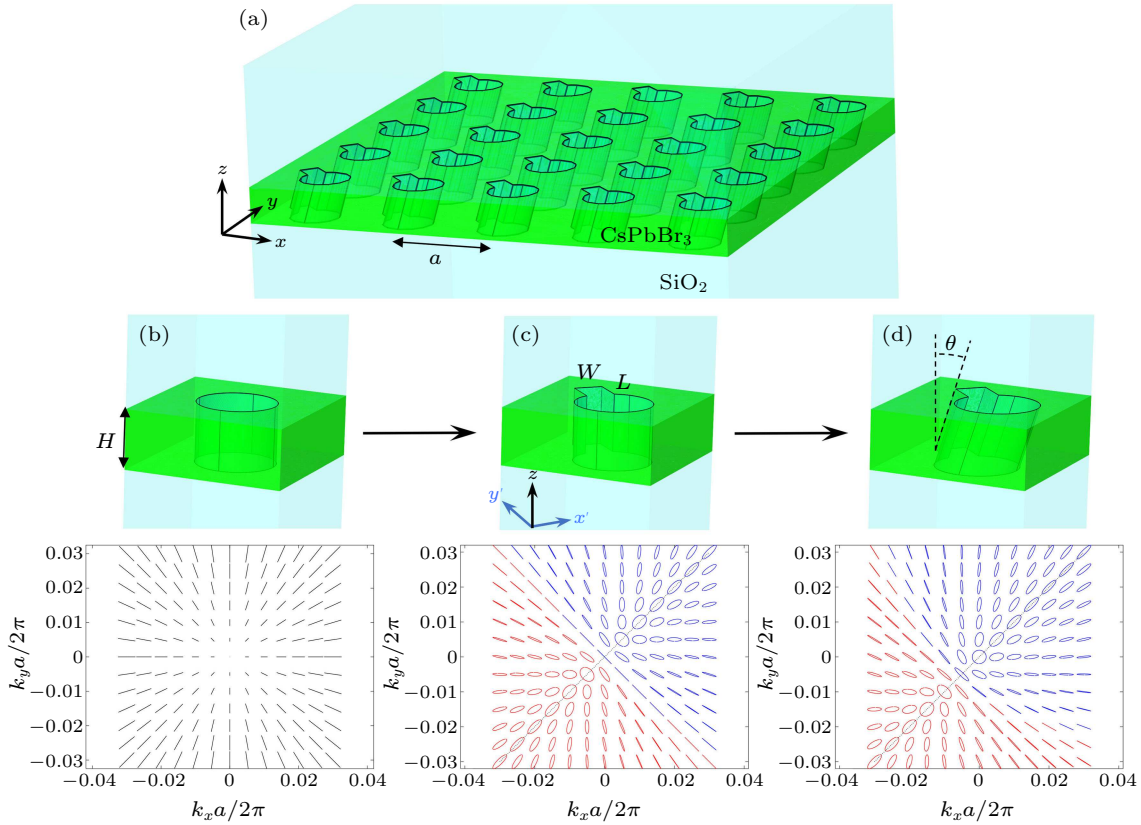


Fig. 1. Illustration of our design and evolution of eigenpolarization maps. (a) Schematic of the designed $CsPbBr_3$ metasurface. Starting from a square array of circular holes (b), a rectangular protrusion is added to the hole (c), and the whole structure is tilted along the 45° direction in xy plane (d). Eigen-polarization maps in momentum space of the corresponding geometry are displayed in the bottom row.

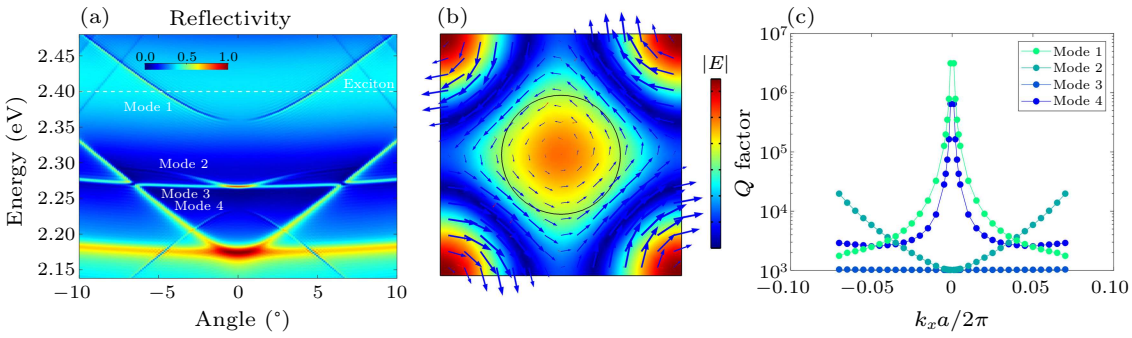


Fig. 2. BIC mode in the unperturbed metasurface. (a) Angle-resolved reflection spectrum of the unperturbed metasurface. Four photonic modes are labeled with decreasing energy. (b) Electric and magnetic field distribution of mode 1 at 0°. (c) Q factors of the four modes in (a).

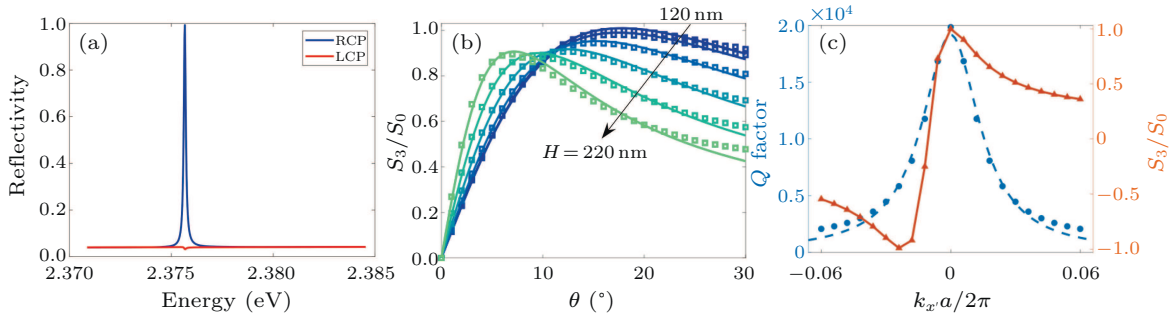


Fig. 3. Intrinsic chiral response of the chiral BIC and its evolution with various parameters. (a) Reflection spectrum at normal incidence, tilting angle $\theta = 18°$. (b) Evolution of S_3/S_0 with angle θ and thickness H. Solid lines are fitting to Eq. (1) in the text. (c) Q factor and S_3/S_0 distribution along x' direction.

As reported in the literature, breaking both in-plane C_2^z and out-of-plane M_z symmetries leads to generation of intrinsic chirality when one of the chiral BIC points in reciprocal space is formed at Γ point. When this happens, the two circular polarization eigenstates are nondegenerate in both energy and momentum, and strong chirality can be accessed at normal incidence. In our design, the optimal perturbation parameters are found to be $W = 60$ nm, $L = 70$ nm, and $\theta = 18°$. Evolution of the eigen-polarization map of mode 1 when the perturbations are added is shown in the bottom panels of Figs. 1(b)–1(d). The BIC singularity at Γ splits into two chiral BICs along x' when the rectangular slot is introduced, and the RCP point further moves to Γ point when the hole is tilted. The reflection spectrum at normal incidence shown in Fig. 3(a) features a sharp peak appearing near 2.375 eV for RCP, with the reflectivity peak value approaching 1 with a full width at half maximum of less than 0.2 meV. By comparison, the resonant response for LCP is very weak, showing a distinguished chiral response. Calculations for different geometries reveal that the intrinsic chirality produced by this strategy is related to the thickness of the metasurface. Figure 3(b) plots the magnitude of normalized Stokes parameter $S_3/S_0 = (I_{\mathrm{RCP}} - I_{\mathrm{LCP}})/(I_{\mathrm{RCP}} + I_{\mathrm{LCP}})$ at Γ with different tilting angle θ and thickness H, with other geometric parameters unchanged. At the current thickness $H = 120$ nm, S_3/S_0 can reach a maximum value of 1 at $\theta = 18°$. As H is gradually increased to 220 nm, the maximum of S_3/S_0 decreases and can no longer reach unity, and its variation also happens at smaller θ, which indicates an increased sensitivity with tilting angle when the structure grows higher. Figure 3(c) plots the change of Q value and S_3/S_0 against the in-plane momentum $k_{x'}$ along x'. The strongest chirality $S_3/S_0 > 0.99$ and a high Q value of 19180 are achieved simultaneously at Γ for RCP while the LCP eigenstate at $k_{x'}a/2\pi \simeq -0.02$ shows a much lower $Q = 5000$, as the Q factor of qBIC is inversely proportional to the weighted sum of squares of each perturbation (fitted blue broken line in Fig. 3(c)): $Q = 1/(|\alpha|^2 + B|k_{x'}|^2)$, where α represents the perturbation from rectangular hole and tilting and B is a measure of relative sensitivity between different perturbations.

Multipole expansion is a technique frequently used to analyze localized electromagnetic fields. In this approach, the induced polarization field $\boldsymbol{P}(\boldsymbol{r})$ and scattering cross section σ_{sca} are decomposed into contributions from multipole moments, with the advantage of approximating fields in complex geometry by familiar low-order moments. Under RCP luminance, the chiral BIC scattering efficiency, defined as $\sigma_{\mathrm{sca}}/(\pi a^2)$, is decomposed to the third order, as shown in Fig. 4(a). The resonance is clearly governed by the toroidal dipole (TD), whose scattering efficiency is an order of magnitude higher than the rest multipoles. In a typical TD resonance, the electric field circles radially across the torus surface, and the magnetic field circulates along the equator. The electric field in the $y'z$ plane and magnetic field in the xy plane at resonant energy are shown in Fig. 4(b). Electric currents flow in a circular pattern between the hot spots, and the magnetic field forms vortices around unit

cell corners, which is characteristic of the TD resonance. In previous works, chiral BIC was mostly produced by the interaction of multiple electric dipoles (ED) within a unit cell[24,27] or by the interaction of electric and magnetic dipoles (MD),[26] relying on the degree of circular polarization (DCP), under the dipole approximation, being proportional to the in-plane overlap of dipole moments; now we have demonstrated that higher-order moments, in particular the TD moment, can also underly a chiral BIC. Multipole theory states that a TD produces similar far-field patterns as an ED,[40] thus we can use the same expression derived under dipole approximation for the DCP or S_3:[26]

$$|S_3/S_0| \propto \frac{\sin\theta}{1+\beta\sin^2\theta}, \tag{1}$$

where β is a fitting parameter describing the dependence of Q factor on θ. Equation (1) is used to fit the curves in Fig. 3(b); this expression holds true despite the electric octupole (EO) being on the same order as MD in Fig. 4(a). It is worth mentioning that recently giant chiral response empowered by TD resonances has also been reported in other structures,[41] implying further applications of the TD in chiral optics.

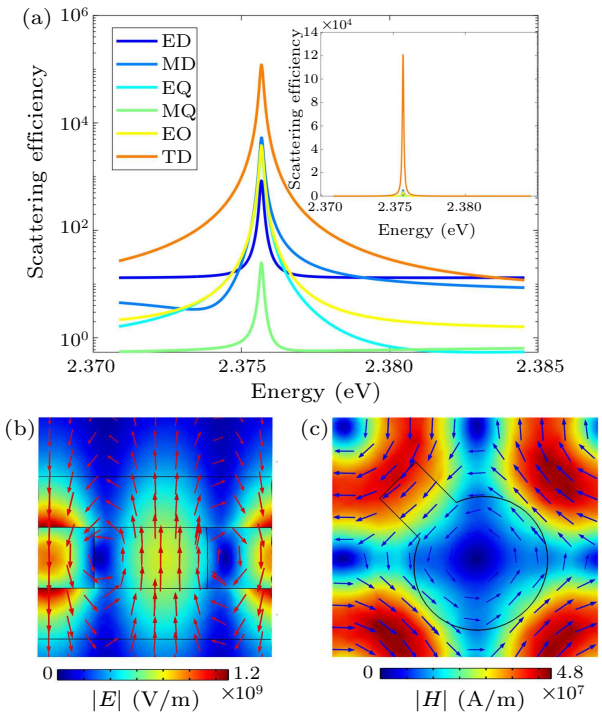


Fig. 4. Multipole analysis of the chiral BIC. (a) Multipole expansion of scattering efficiency at the chiral BIC resonance. ED, electric dipole; MD, magnetic dipole; EQ, electric quadrupole; MQ, magnetic quadrupole; EO, electric octupole; TD, toroidal dipole. Inset is the same plot in linear scale. (b) $x'z$ plane cut of the electric field distribution. (c) xy plane cut of the magnetic field distribution.

3. Intrinsic chiral BIC exciton polaritons

In this section, we incorporate the exciton contribution into the $CsPbBr_3$ refractive index by using measured values from the literature.[39] $CsPbBr_3$ belongs to the family of lead halide perovskites, which are direct bandgap semiconductors with bandgaps that can be tuned by adjusting the chemical composition. They possess high optical gain, large oscillator strength, and considerable flexibility in growth techniques. As a result, there has been an ongoing perovskite fever in the field of optoelectronics and especially, lead halide perovskites provide an excellent platform for exciton polariton research.[31,38,42] The Wannier–Mott exciton binding energy in $CsPbBr_3$ is 40 meV,[38] allowing excitons to exist stably at room temperature, opening up possibilities for room-temperature devices.

Here we calculate the angle-resolved absorption spectrum of the $CsPbBr_3$ chiral BIC metasurface under circularly polarized light. As the structure no longer possesses C_4^z symmetry, spectra resolved along x' and y' directions are respectively calculated, as shown in Fig. 5. The exciton energy in $CsPbBr_3$ is $E_X = 2.407$ eV (shown as the white broken line in Fig. 5). Above this energy there is strong absorption, thus only the lower polariton branch (LPB) can be clearly seen. We use the coupled oscillator model to fit the strong coupling between photons and excitons:

$$H\psi = E_{\mathrm{LPB/UPB}}\psi, \text{ where } H = \begin{pmatrix} E_p(k_{||}) & g \\ g^* & E_X \end{pmatrix}, \tag{2}$$

where $k_{||}$ is the in-plane wavevector, $E_p(k_{||})$ is the photon dispersion given in the passive calculations, and g is the coupling strength. The solution of Eq. (2) gives the polariton dispersion relations

$$E_{\mathrm{LPB/UPB}}(k_{||}) = \frac{1}{2}(E_p(k_{||}) + E_X(k_{||}) \pm \sqrt{(E_p(k_{||}) - E_X(k_{||}))^2 + 4|g|^2}). \tag{3}$$

In our calculations, the detuning is $\Delta(0) \equiv E_p(0) - E_X(0) = -36$ meV and the Rabi splitting is $|2g| = 103.1$ meV. As shown in Figs. 5(a) and 5(b), along x' direction at the angles around -2° RCP becomes a dark state with a linewidth reducing to zero, corresponding to a LCP chiral eigenstate, and LCP at around 0.5°, indicating that the chirality is preserved in the dispersion of exciton polaritons. The intrinsic chiral BIC of RCP does not seem to be centered at 0°, because the eigenpolarization distribution is not centrosymmetric with respect to Γ(Figs. 1(d) and 3(c)); stronger RCP chirality is maintained along the $k_{x'} > 0$ direction. Nevertheless, chirality at the Γ point can still be observed in the LPB, as shown in Fig. 5(c). Here, the degree of circular polarization (DCP) is defined as $\mathrm{DCP} = (A_{\mathrm{LCP}} - A_{\mathrm{RCP}})/(A_{\mathrm{LCP}} + A_{\mathrm{RCP}})$, where $A_{\mathrm{L(R)CP}} = 1 - T_{\mathrm{L(R)CP}} - R_{\mathrm{L(R)CP}}$ is the absorption under LCP (RCP) calculated from the transmittance and reflectivity. The $k_x < 0$ and $k_x > 0$ regions of LPB exhibit distinct chiral responses over a large angular range, and at 0° incidence a sharp DCP peak appears near 2.29 eV with a peak width of only

0.4 meV, corresponding to $Q = 7434$, which clearly demonstrates the intrinsic chirality of exciton polaritons. For comparison, the other DCP peak at lower energy shows weaker chirality and broader linewidth, which originates from the non-BIC mode 2 (see Fig. 2(a)).

Figures 5(d) and 5(e) show the corresponding absorption spectrum resolved along y' direction. The effective mass of photons in the y' direction is slightly smaller than that in the x' direction ($m_{y'}^{\mathrm{eff}}/m_{x'}^{\mathrm{eff}} = 0.87$), other than which there is no significant difference in the energy-momentum dispersion of the LPB. However, its coupling with circularly polarized light is drastically different. According to the eigen-polarization mapping in Fig. 1(d), the eigenstate quickly becomes linearly polarized when moving away from the Γ point along y', which couples equally to LCP and RCP, so the chiral signal of the RCP eigenstate should only appear in a small angular region near the Γ point. In Figs. 5(d) and 5(e), the LPB under RCP has a reduced (but not zero) linewidth at 0°, behaving as a quasi-BIC, while LCP shows a complete BIC dark state at 0°. The region near $k_{y'} = 0$, indicated by the black arrow in Fig. 5(f), with an angular width of approximately 2°, exhibits nonnegligible DCP which corresponds to the RCP chiral BIC, while the chirality is weaker at other angles on this branch. This result of intrinsic chirality breaks the degeneracy between LCP and RCP in both energy and momentum spaces.

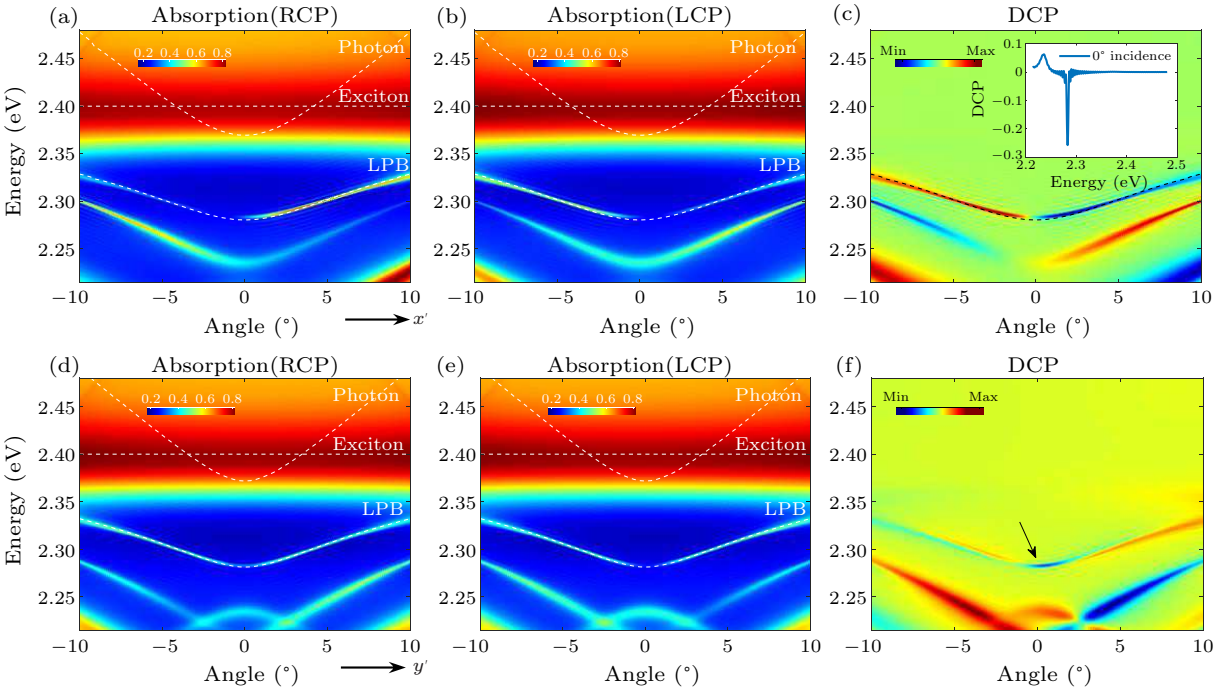


Fig. 5. Angle-resolved spectra of chiral BIC exciton polaritons. (a) and (b) Angle-resolved absorption spectra along x' axis under RCP and LCP incidence. White dashed lines are fits to the coupled oscillator model. (c) DCP along x' axis calculated from the absorption spectrum. Inset shows the line cut at the normal incidence. (d) and (e) Angle-resolved absorption spectra along y' axis. (f) DCP along y' axis calculated from the absorption spectrum.

To study the photoluminescence (PL) of the exciton polariton in the linear region, we can invoke the reciprocity principle in electrodynamics.[43] With this tool, we can estimate how the PL intensity is boosted by evaluating the integration of electric field strength in the active region. Reciprocity states that any two harmonic current sources $\boldsymbol{j}_{1,2}(\boldsymbol{r})$ and the electric fields $\boldsymbol{E}_{1,2}(\boldsymbol{r})$ produced by them must satisfy the relation $\int \boldsymbol{j}_1 \cdot \boldsymbol{E}_2 \,\mathrm{d}V = \int \boldsymbol{j}_2 \cdot \boldsymbol{E}_1 \,\mathrm{d}V$. If we take subscript 1 as the incident light field and model the PL as emission from randomly placed dipole sources $\boldsymbol{j}_2 = -\mathrm{i}\omega \sum_m \boldsymbol{p}_m \delta(\boldsymbol{r} - \boldsymbol{r}_m)$, then the emitted field $\boldsymbol{E}_2$ can be simply evaluated by integrating $\boldsymbol{E}_1$ inside the perovskite region,[33] and an enhancement factor F can be defined against the incident plane wave amplitude E_{inc} as $F = \int |\boldsymbol{E}_1(\boldsymbol{r})| \mathrm{d}V / \int E_{\mathrm{inc}} \mathrm{d}V$. On this basis, we calculate the angle-resolved PL enhancement factor along the x' and y' directions under LCP or RCP incidence, as shown in Figs. 6(a)–6(f). Along x', left and right circularly polarized light can provide an enhancement of 80 to 100 times at certain angles, respectively, and has DCP (calculated from emission) as high as 95% at the chiral BIC points. Note that the large DCP broadening in Figs. 6(c) and 6(f) does not represent the actual linewidth of the polariton emission; DCP is independent of the absolute intensity of PL. Along the y' direction, chiral PL enhancement only occurs at the Γ point, as indicated by the arrow in Fig. 6(f). The highest gain does not happen at Γ where the Q factor is the largest, but rather at a slightly higher energy with nonzero momentum. It has been shown[33] that when both radiative and non-radiative decay channels γ_{r} and γ_{nr} exist, the largest gain occurs at the so-called critical coupling point, satisfying $\gamma_{\mathrm{r}} = \gamma_{\mathrm{nr}}$. Although the LPB bottom is

some distance away from the absorption edge of $CsPbBr_3$ exciton, previous calculations have shown that there is a uniform polarization-independent background absorption of about 0.1 in this range, therefore the chiral BIC state which has quite a long radiative lifetime does not satisfy the critical coupling criterion. Moving away from Γ, the Q factor decreases, γ_r increases until it equals the absorption-induced γ_{hr}, at which point the gain is maximized, at an angle of approximately $\pm 5°$. Further increasing the angle will again go away from the critical coupling point and result in decreased gain. Taking into consideration that a polariton condensate will occur at the point of maximum gain,[44] this result may suggest that condensation on a finite momentum state will occur in this chiral BIC system. Such a condensate will have the advantages of both chirality-tunability and ultrafast propagation.

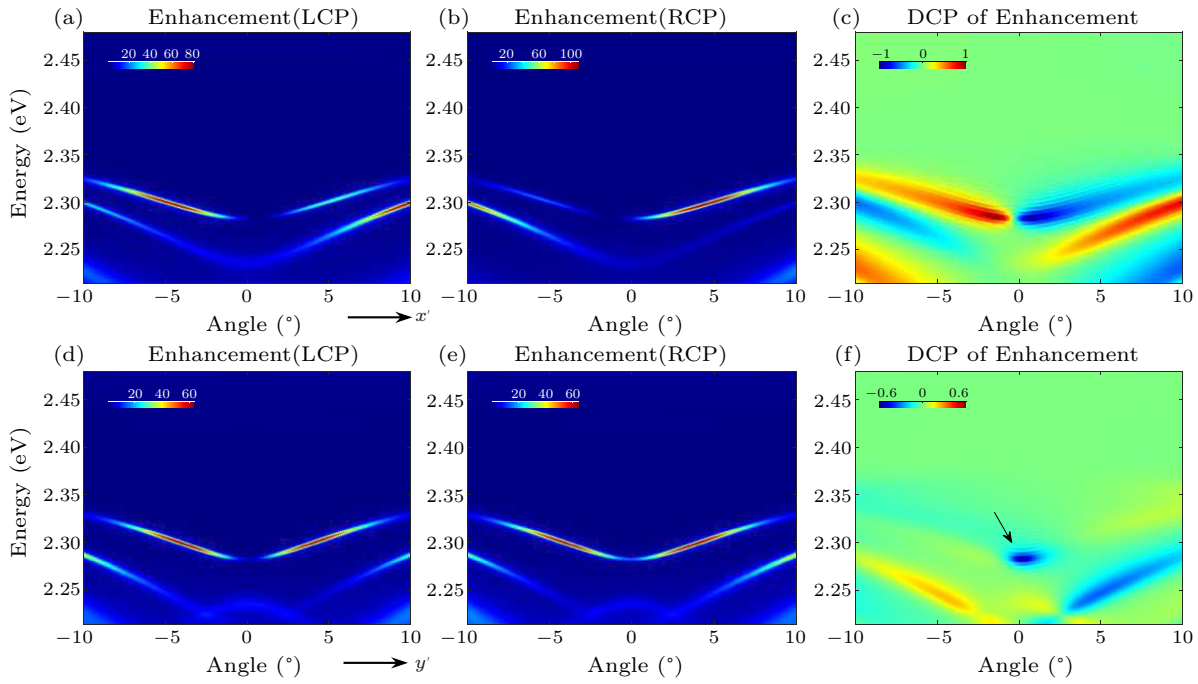


Fig. 6. Photoluminescence enhancement by the chiral BIC. (a) and (b) PL enhancement under LCP and RCP resolved along x' axis, calculated using the reciprocal relation. (c) DCP of PL enhancement along x' axis. (d) and (e) PL enhancement of LCP and RCP resolved along y' axis. (f) DCP of PL enhancement along y' axis.

4. Conclusion and perspectives

The pursuit of novel chiral light sources holds great significance for both fundamental physics and device applications. In this work, we propose a scheme to generate pure, directional and high Q chiral light from exciton polaritons, using the physics of bound states in the continuum. We numerically designed a two-dimensional perovskite metasurface supporting a chiral BIC. The true BIC is transformed into a chiral BIC by implementing in-plane and out-of-plane geometric perturbations that disrupt the symmetry between the two circular polarizations. By optimizing parameters such as inclination angle and height, a high Q factor exceeding 20000 and intrinsic chirality $|S_3/S_0| > 0.99$ are simultaneously achieved at normal incidence. Furthermore, calculations extended to the third-order multipole decomposition revealed that the chiral BIC primarily originates from the resonant toroidal dipole moment, transcending the conventional dipole approximation. Through calculation of angle-resolved absorption spectrum with exciton contribution to the refractive index of $CsPbBr_3$ included, we confirmed strong coupling between excitons and photons with a Rabi splitting of 103.1 meV and clarified the intrinsic chiral response of the exciton polaritons. Applying the principle of reciprocity, we simulated the linear PL of the perovskite metasurface, showcasing the strongly polarization-dependent enhancement of exciton polariton emission by the chiral BIC. The emitted light at specific angles exhibited a DCP of 0.95, and the intrinsic RCP emission enhancement at Γ also achieved a DCP higher than 0.6.

Experimentally, this structure could be fabricated using slanted etching setups similar to those described in literature,[26,27] followed by thickness-controlled growth of perovskite.[45] The resolution on the order of 10 nm required for this task is challenging but worth further research. Our design provides a practical path to exciton polariton based chiral optics and has potential applications in high-purity chiral light sources and polarization-resolved ultrafast optical switches. From the perspective of fundamental physics, the condensation dynamics of polaritons with different chirality is also waiting for further exploration. Thus, our results hold great significance for chiral optics and light–matter interactions.

Acknowledgments

D. W. thanks Dr. Tengfei Li for helpful discussions on FEM simulations. Q. X. gratefully acknowledges the strong funding support from the National Key Research and Development Program of China (Grant No. 2022YFA1204700) and the National Natural Science Foundation of China (Grant Nos. 12020101003, 92056204, and 92250301). S. G. acknowledges the funding support from the National Natural Science Foundation of China (Grant No. 12274034).

References

[1] Du W, Wen X, Gérard D, Qiu C W and Xiong Q 2019 *Sci. China Phys. Mech. Astron.* **63** 244201
[2] Parappurath N, Alpeggiani F, Kuipers L and Ewold V 2020 *Sci. Adv.* **6** eaaw4137
[3] Lodahl P, Mahmoodian S, Stobbe S, Rauschenbeutel A, Schneeweiss P, Volz J, Pichler H and Zoller P 2017 *Nature* **541** 473
[4] Schaibley JR, Yu H, Clark G, Rivera P, Ross J S, Seyler K L, Yao W and Xu X 2016 *Nat. Rev. Mater.* **1** 16055
[5] Whittaker P, Kloner R A, Boughner D R and Pickering J G 1994 *Basic Res. Cardiol.* **89** 397
[6] Li J, Schuster G B, Cheon K S, Green M M and Selinger J V 2000 *J. Am. Chem. Soc.* **122** 2603
[7] Chen Y, Du W, Zhang Q, Ávalos-Ovando O, Wu J, Xu Q H, Liu N, Okamoto H, Govorov A O, Xiong Q and Qiu C W 2022 *Nat. Rev. Phys.* **4** 113
[8] Huang Y, Polojärvi V, Hiura S, Höjer P, Aho A, Isoaho R, Hakkarainen T, Guina M, Sato S, Takayama J, Murayama A, Buyanova I A and Chen W M 2021 *Nat. Photonics* **15** 475
[9] Wang Y, Zheng H, Tang Z, Wang R, Luo X, Shen Y, Yang X, Liu K K, Wang S, Deng S, Shan C X and Zhu H 2023 *ACS Photonics* **10** 1936
[10] Nishizawa N, Nishibayashi K and Munekata H 2017 *Proc. Natl. Acad. Sci. USA* **114** 1783
[11] Zhang Z, Fan F, Li T, Ji Y and Chang S 2020 *Chin. Phys. B* **29** 78707
[12] Shi T, Deng Z L, Geng G, Zeng X, Zeng Y, Hu G, Overvig A, Li J, Qiu C W, Alù A, *et al.* 2022 *Nat. Commun.* **13** 4111
[13] Chen Y, Feng J, Huang Y, Chen W, Su R, Ghosh S, Hou Y, Xiong Q and Qiu C W 2023 *Nat. Mater.* **22** 1065
[14] Rong K, Duan X, Wang B, Reichenberg D, Cohen A, Liu C L, Mohapatra P K, Patsha A, Gorovoy V, Mukherjee S, Kleiner V, Ismach A, Koren E and Hasman E 2023 *Nat. Mater.* **22** 1085
[15] Hsu C W, Zhen B, Stone A D, Joannopoulos J D and Soljačić M 2016 *Nat. Rev. Mater.* **1** 16048
[16] Yin X, Jin J, Soljačić M, Peng C and Zhen B 2020 *Nature* **580** 467
[17] Wang B, Liu W, Zhao M, Wang J, Zhang Y, Chen A, Guan F, Liu X, Shi L and Zi J 2020 *Nat. Photonics* **14** 623
[18] Wang J, Shi L and Zi J 2022 *Phys. Rev. Lett.* **129** 236101
[19] Jiang X, Fang B and Zhan C 2024 *Chin. Phys. B* **33** 34206
[20] Tang H, Hu P, Cui D J, Xiang H and Han D 2022 *Chin. Phys. B* **31** 104209
[21] Bernhardt N, Koshelev K, White S J U, Meng K W C, Froch J E, Kim S, Tran T T, Choi D Y, Kivshar Y and Solntsev A S 2020 *Nano Lett.* **20** 5309
[22] Zhen B, Hsu C W, Lu L, Stone A D and Soljacic M 2014 *Phys. Rev. Lett.* **113** 257401
[23] Lim Y, Seo I C, An S C, Kim Y, Park C, Woo B H, Kim S, Park H R and Jun Y C 2022 *Laser Photonics Rev.* **17** 2200611
[24] Gorkunov M V, Antonov A A and Kivshar Y S 2020 *Phys. Rev. Lett.* **125** 093903
[25] Liu W, Wang B, Zhang Y, Wang J, Zhao M, Guan F, Liu X, Shi L and Zi J 2019 *Phys. Rev. Lett.* **123** 116104
[26] Chen Y, Deng H, Sha X, Chen W, Wang R, Chen Y H, Wu D, Chu J, Kivshar Y S, Xiao S and Qiu C W 2023 *Nature* **613** 474
[27] Zhang X, Liu Y, Han J, Kivshar Y and Song Q 2022 *Science* **377** 1215
[28] Yang J, Shi A, Peng Y, Peng P and Liu J 2024 *Chin. Phys. B* **33** 084206
[29] Muhammad N, Chen Y, Qiu C W and Wang G P 2021 *Nano Lett.* **21** 967
[30] Liu X J, Yu Y, Liu D, Cui Q L, Qi X, Chen Y, Qu G, Song L, Guo G P, Guo G C, *et al.* 2023 *Nano Lett.* **23** 3209
[31] Ghosh S, Su R, Zhao J, Fieramosca A, Wu J, Li T, Zhang Q, Li F, Chen Z, Liew T, Sanvitto D and Xiong Q 2022 *Photonics Insights* **1** R04
[32] Koshelev K L, Sychev S K, Sadrieva Z F, Bogdanov A A and Iorsh I V 2018 *Phys. Rev. B* **98** 161113
[33] Kim S, Woo B H, An S C, Lim Y, Seo I C, Kim D S, Yoo S, Park Q H and Jun Y C 2021 *Nano Lett.* **21** 10076
[34] Al-Ani I A M, As'Ham K, Huang L, Miroshnichenko A E, Lei W and Hattori H T 2022 *Adv. Opt. Mater.* **10** 2101120
[35] Ardizzone V, Riminucci F, Zanotti S, Gianfrate A, Efthymiou-Tsironi M, Suarez-Forero D G, Todisco F, De Giorgi M, Trypogeorgos D, Gigli G, Baldwin K, Pfeiffer L, Ballarini D, Nguyen H S, Gerace D and Sanvitto D 2022 *Nature* **605** 447
[36] Berghuis A M, Castellanos G W, Murai S, Pura J L, Abujetas D R, Heijst E, Ramezani M, Sánchez-Gil J A and Rivas J G 2023 *Nano Lett.* **23** 5603
[37] Wu X, Zhang S, Song J, Deng X, Du W, Zeng X, Zhang Y, Zhang Z, Chen Y, Wang Y, *et al.* 2024 *Nat. Commun.* **15** 3345
[38] Su R, Fieramosca A, Zhang Q, Nguyen H S, Deleporte E, Chen Z, Sanvitto D, Liew T C H and Xiong Q 2021 *Nat. Mater.* **20** 1315
[39] Ermolaev G, Pushkarev A P, Zhizhchenko A, Kuchmizhak A A, Iorsh I, Kruglov I, Mazitov A, Ishteev A, Konstantinova K, Saranin D, Slavich A, Stosic D, Zhukova E S, Tselikov G, Di Carlo A, Arsenin A, Novoselov K S, Makarov S V and Volkov V S 2023 *Nano Lett.* **23** 2570
[40] Evlyukhin A B, Fischer T, Reinhardt C and Chichkov B N 2016 *Phys. Rev. B* **94** 205434
[41] Wu J, Jiang H, Guo Z, Sun Y, Li Y and Chen H 2023 *Opt. Lett.* **48** 916
[42] Su R, Diederichs C, Wang J, Liew T C H, Zhao J, Liu S, Xu W, Chen Z and Xiong Q 2017 *Nano Lett.* **17** 3982
[43] Balanis C A 2012 *Advanced Engineering Electromagnetics* 2nd Edn. (Hoboken, New Jersey: John Wiley & Sons) p. 323
[44] Su R, Ghosh S, Wang J, Liu S, Diederichs C, Liew T C H and Xiong Q 2020 *Nat. Phys.* **16** 301
[45] Chen Y X, Ge Q Q, Shi Y, Liu J, Xue D J, Ma J Y, Ding J, Yan H J, Hu J S and Wan L J 2016 *J. Am. Chem. Soc.* **138** 16196